



Cite this: *Nanoscale*, 2025, **17**, 10187

Low-threshold colloidal quantum dot polariton lasing *via* a strong coupling microcavity at room temperature†

Junxing Dong,^a Yuting Wu,^b Runchen Wang,^a Lisheng Wang,^a Jingzhuo Wang,^a Yifan Zhang,^a Yue Wang,^{*b} Xianghu Wang,^c Si Shen^{*d} and Hai Zhu  ^{*a}

Colloidal quantum dots (CQDs) are excellent optical gain media that can be synthesized through low-cost and easily controlled techniques, holding significant promise for applications in semiconductor laser devices. In this study, we demonstrated polariton coherent lasing based on a CdSe-based CQD microcavity device at room-temperature (RT) for the first time. The dispersion behaviors of CQD polaritons with different excitation powers were comprehensively analyzed using angle-resolved spectroscopy techniques. The lasing behavior at a threshold of $49 \mu\text{J cm}^{-2}$ and the energy blue-shift were well aligned with the typical characteristics of robust polariton Bose–Einstein condensation (BEC) theory. Moreover, the linewidth of the polariton lasing peak was narrowed down to 0.65 nm at $1.13P_{\text{th}}$. Additionally, the polarization characteristics and temporal dynamics of the CQD-microcavity polariton lasing were discussed. It was noted that the lifetime of CQD polaritons during condensation was reduced from 1.3 ns ($0.8P_{\text{th}}$) to 68 ps ($1.6P_{\text{th}}$). Our results provide valuable insights into the strong coupling, low-threshold CQD microcavity laser at RT and promote its further practical application.

Received 9th December 2024,

Accepted 28th February 2025

DOI: 10.1039/d4nr05185h

rsc.li/nanoscale

Low-dimensional quantum confinement semiconductor materials have played important roles in fields such as nanophotonics and novel optoelectronic devices.¹ For quantum confinement in all three dimensions, a quantum dot (QD) active medium will be constructed. Colloidal quantum dots are typical artificial QD media that can be synthesized and manipulated through low-cost and controllable fabrication techniques.² Due to their solution dispersibility, CQDs are substrate-independent and compatible with various optical resonant cavities, thereby offering enormous potential for the development of micro laser devices.³ Theoretically, CQDs have lower lasing thresholds and higher gain coefficients than bulk semiconductor materials.^{4,12} In practice, amplified spon-

aneous emission and lasing have been reported using several types of cavities, including distributed Bragg reflectors (DBRs), distributed feedback gratings and micro-rings.^{5–11} To further reduce the lasing threshold of CQDs, the strong coupling effect between CQD excitons and microcavity photons has been proposed. In this scheme, the QDs can reabsorb emitted photons before they leak out, forming exciton–polariton states. A few researchers have discussed the coherent radiation of QD exciton-polaritons under low-temperature conditions.^{13,14} However, due to significant thermal diffusion caused by the optical gain of QDs as the temperature increases, the strong coupling system of quantum dots in the RT range faces many limitations. Currently, although CQD lasers with resonant cavity structures optically pumped have been reported, there is still a lack of work on the realization of CQD polariton lasing in strong coupling microcavities at RT, which could provide important references for QD lasers at ultra-low thresholds. Therefore, the optimum design of the microcavity and the uniformity of CQDs are critical factors for realizing polariton lasers.

In this study, we achieved RT polariton condensation lasing of CdSe/ZnSe/ZnS CQDs *via* a two-dimensional strong coupling vertical microcavity configuration constructed with pairs of DBRs. Based on the strong coupling between the biexciton state and the designed cavity mode, the polariton system exhibits a Rabi splitting of 45 meV. As the optical excitation power

^aState Key Laboratory of Optoelectronic Materials and Technologies, School of Physics, Sun Yat-Sen University, Guangzhou 510275, China.

E-mail: zhuohai5@mail.sysu.edu.cn

^bCollege of Materials Science and Engineering, Nanjing University of Science and Technology, Nanjing 210094, China. E-mail: ywang@njust.edu.cn

^cSchool of Materials, Shanghai Dianji University, Shanghai 200245, China

^dEast China Normal University, Shanghai, 200241, China.

E-mail: sshen@lps.ecnu.edu.cn

†Electronic supplementary information (ESI) available: Additional descriptions of the CQD synthesis method, the reflectance spectrum of the DBRs, the morphology of the CQDs spin-coated on the DBR surface, a simplified experimental setup and theoretical descriptions of the strong-coupled system in the planar microcavity. See DOI: <https://doi.org/10.1039/d4nr05185h>



density increases, the device's output signal underwent a transition from fluorescence to lasing emission, exhibiting energy condensation above the threshold towards small angles, as well as an emission peak energy blue-shift of 3.1 meV below the threshold, which is consistent with the behavior of polariton BEC. Additionally, the lifetime decay mechanism and polarization properties of the quantum dot lasers were investigated. The CQDs exhibited emission lifetime reduction to 1/50 above the threshold and showed weak polarization throughout the entire process. These results validate the feasibility of achieving CQD polariton condensation lasing at RT through the strong coupling microcavities and pave the way for the practical application of ultra-low threshold CQD polariton laser devices.

The schematic of the CQD microcavity device is given in Fig. 1a. The top and bottom sections of the microcavity were composed of DBRs. A 0.8 μm -thick CdSe/ZnSe/ZnS CQDs layer was deposited on the bottom DBR *via* spin coating, followed by the transfer of the top DBR onto this assembly. The CdSe/ZnSe/ZnS core/shell/shell structure provided high photoluminescence quantum yield and excellent photostability owing to the intermediate ZnSe shell that relieves lattice strain and the outer ZnS shell that offers additional protection.¹⁵ The high reflectivity of the DBRs layers effectively confines the light field within the microcavity. Notably, the energy of the cavity modes was designed to match the spontaneous emission (SE) from the biexciton transition of CQDs. The microstructure of the CQDs samples was analyzed using transmission electron microscopy (TEM), as shown in the inset of Fig. 1a. The synthesized CdSe/ZnSe/ZnS QDs exhibited a spherical structure with an average particle size of 12.5 nm. To explore the optical properties and energy-momentum dispersion relationship of

the CQD microcavity device, a home-built angle-resolved micro-photoluminescence ($\mu\text{-PL}$) system was adopted.^{16,17} A continuous-wave (CW) white light source was used to excite the sample, and the angle-resolved transmission spectrum was obtained (Fig. 1b). Here, the emission signal from the microcavity could be resolved into k_{\perp} and k_{\parallel} directions, respectively perpendicular and parallel to the microcavity surface. The observed parabolic dispersion pattern indicates that the excitons of the CQDs were strongly coupled with the light field in the planar microcavity.¹⁸

To investigate the energy level of the CdSe/ZnSe/ZnS CQDs, a femtosecond pulsed laser with a central wavelength of 400 nm was used for the optical excitation of the samples. The RT power-dependent photoluminescence spectra of bare CQDs exhibited a typical SE process, as shown in Fig. 1c. At lower excitation power, the peak at 636.5 nm originating from the $|X\rangle \rightarrow |0\rangle$ transition dominated the spectrum.¹⁹ With increasing pumping power, the biexcitonic gain mechanism became operative, and the gain of the $|XX\rangle \rightarrow |0\rangle$ emission (601.6 nm) was the dominant radiation. The energy shift between these two emission bands indicated an X-X interaction energy of 113 meV.

The evolution of polariton distribution in the K-space of CQD-microcavity under different excitation powers was investigated comprehensively. Under low excitation conditions, the dispersion pattern exhibited a typical lower polariton (LP) branch (Fig. 2a). Notably, the upper polariton (UP) branch signal was not observed, which can be attributed to its short lifetime because of the self-absorption effect and strong exciton-phonon interactions at RT.²⁰ In the dispersion pattern, the LP branch fitting curve is represented by the yellow dashed line, while the cavity mode curve is represented

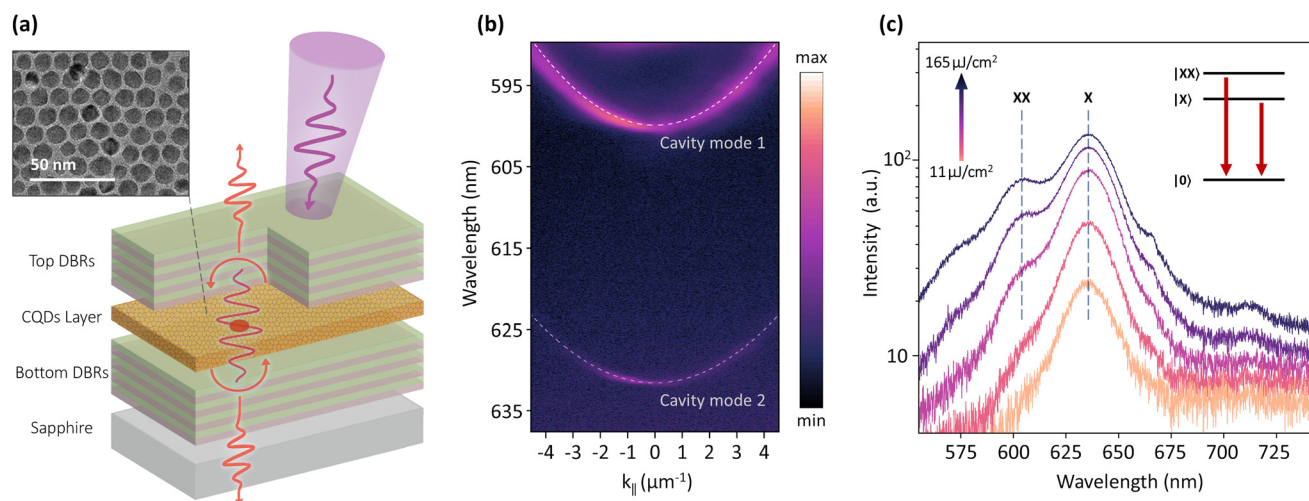


Fig. 1 Design and characterization of the CQDs strong-coupled microcavity. (a) Schematic of the microcavity device. The CdSe-based CQDs act as the gain medium and are positioned between a pair of DBRs, forming a planar microcavity. The sample is pumped with a laser vertically incident from one side. Inset: TEM image of the CQDs sample. (b) Angle-resolved transmission spectra measured at RT under CW resonant excitation in the visible light range. The bright curves in the image represent cavity modes coupling with the active medium. The white dashed lines indicate the fitting. (c) The power-dependent photoluminescence spectra of bare CQDs at RT exhibit two characteristic peaks, corresponding to two emission modes of biexcitons. Inset: Schematic of the biexciton energy level (a.u., arbitrary units).



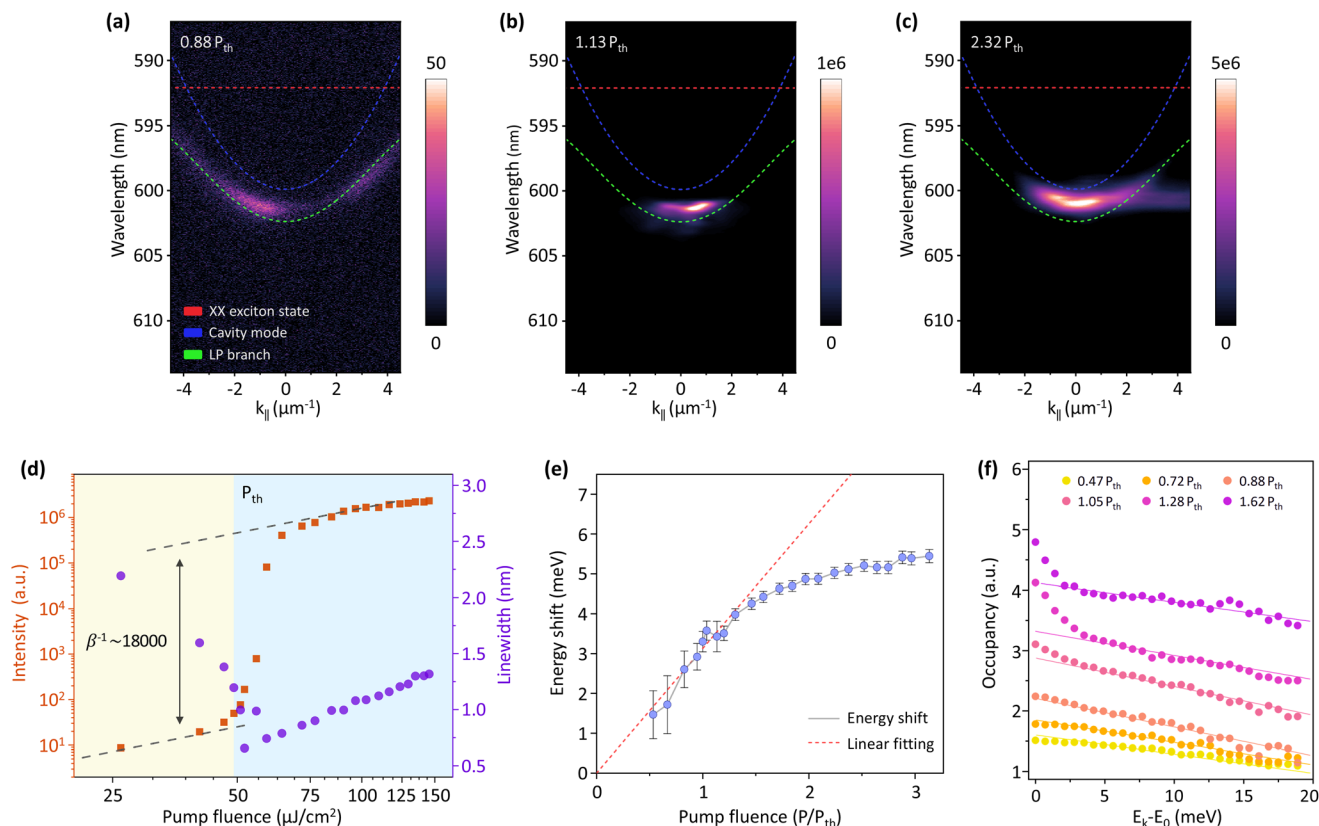


Fig. 2 Power-dependent polariton coherent radiation of the CQD-microcavity at RT. (a) Angle-resolved emission pattern of the LP branch under low excitation power ($0.88 P_{th}$). The pattern displays that polariton particles are broadly distributed in the LP branch. The exciton state, bare cavity mode, and coupled LP mode are indicated. (b) The emission pattern above the critical intensity ($1.13 P_{th}$) shows that a large number of polariton quasi-particles accumulate in the ground state ($E = 0$), and the linewidth of the peak sharply narrows, indicating the BEC phase transition of polaritons. (c) At higher power ($2.32 P_{th}$), the emission linewidth broadens, and the LP exhibits a typical blue shift compared to low excitation power. (d) Integrated intensity and linewidth of polaritons near $E = 0$ as a function of excitation density. Near P_{th} ($49 \mu J cm^{-2}$), emission intensity rises rapidly with a narrowing of the linewidth, indicating the transition from SE to BEC lasing. (e) The relationship between the blue shift of LP energy and excitation density. At low power, the evolution roughly follows a linear trend with a red dashed linear fit. Beyond the critical threshold, the energy shift tends to saturate. The error bars represent the standard deviation of the estimated energy shift. (f) Condensation features of polaritons in different energy states under various excitation powers. Below the threshold, the occupation numbers follow the Maxwell-Boltzmann distribution function (represented by the fitted straight line). Above the threshold, an increase in the ground-state occupation number is observed.

by the blue dashed line (Fig. 2a-c). The actual energy of the |XX> exciton state (red dashed line) was numerically calculated to be 2.09 eV (592 nm) based on the LP branch and cavity mode curves. Further, according to the fitting data, the strong coupling system had a negative detuning of -27 meV, and the Rabi splitting energy was 45 meV. As the excitation power exceeded a critical value ($49 \mu J cm^{-2}$), the polariton quasi-particles accumulated significantly at the ground state in terms of energy and the momentum scale *via* strong correlation interactions (Fig. 2b). The direct insight of polariton concentration towards the $k_{||} = 0$ position in the momentum space indicated the occurrence of BEC transition of polaritons. In this case, the coherence feature of the polariton system was enhanced dramatically. At higher excitation power (Fig. 2c), the LP branch around $k_{||} = 0$ will be massively occupied, and the repulsive interaction between the polariton quasi-particles will be boosted. Consequently, a blue shift and linewidth broadening of the polariton emission peak were seen in the dispersion

pattern. The dependence of emission intensity and linewidth near $k_{||} = 0$ of the LP branch on excitation power is given in Fig. 2d. In the low-power region, the increase in emission intensity exhibited an almost linear relationship with the excitation power. Meanwhile, the narrowing of the polariton linewidth indicated the establishment of coherent properties.²¹ Near the condensation threshold, the emission intensity of LP increased sharply, and the emission intensity was strongly enhanced. The linewidth of the emission peak reduced to about 0.65 nm, which indicates that the polaritons transit into a nonlinear regime according to the formula

$$Q = \lambda_0 / \Delta\lambda$$

where λ_0 is the central wavelength, and $\Delta\lambda$ is the linewidth. The Q -factor of the fabricated CQD-microcavity was calculated to be about 930. Along with the phase transition of the polariton system above the threshold, the emission intensity of BEC lasing *versus* input power showed linear growth action. The



analysis of the power dependence yielded a spontaneous-emission coupling factor of $\beta \sim (18\,000)^{-1}$ for the polariton laser, representing the proportion of spontaneously emitted polaritons that enter the stimulated scattering mode.²⁴ Compared with conventional microcavity lasers, the factor β of polariton lasers can be much lower (the former generally exceeds 0.01). This is because polariton lasers do not require particle number inversion but achieve lasing when the number of ground-state occupying polariton quasi-particles exceed the threshold.

The blue shift of the ground state energy of the LP branch is a unique aspect of exciton-polaritons and originates from its boson statistics. The noticeable overall increase in the polariton ground-state energy is clear evidence of the repulsive LP-LP interaction in the strong coupling regime.^{16,23} The relationship between the energy shift and excitation power density is presented in Fig. 2e. In the low-excitation-intensity region, the energy of the polaritons can be calculated using mean-field approximation. The energy shift ΔE is nearly linear to the density of polaritons n , which is given by

$$\Delta E = gn$$

Here, factor g represents the interaction strength between the polariton quasi-particles.²⁰ Above the P_{th} , the LP-LP correlation interactions become stronger in the phase space. Hence, the Bose-Einstein distribution of polaritons no longer adequately describes the experimental data. In this situation, the many-body correlation interactions among polariton particles cause the diminution of the energy shift.

Subsequently, we calculated the occupation numbers of polaritons across different energy states under various excitation powers (Fig. 2f). Below the threshold, the occupation number of polaritons can be accurately described by a single

exponential decay function, consistent with Maxwell-Boltzmann distribution at the thermal equilibrium.^{20,23} The fitting results are indicated by the dashed lines in the figure. When the excitation power exceeded the threshold, an upturn in the distribution of polaritons at the ground state was observed, suggesting a deviation from Maxwell-Boltzmann statistics, and the particle distribution gradually approached the Bose-Einstein distribution.

In order to explore the emission properties of the polaritons in the CQD-microcavity comprehensively, the spectra integrated over all $k_{||}$ directions under different excitation conditions were obtained (Fig. 3a). At low input powers, a weak spontaneous emission band was seen in the spectrum. Noticeably, the single-mode lasing peak dominated the spectra as the excitation power exceeded the critical threshold. Near-field images showed a weak emission image in real space from the CQD-microcavity at a low power of $0.6P_{th}$ (Fig. 3b). However, the bright emission spot for the spatial distribution of polaritons was significantly enhanced at high excitation powers (Fig. 3c and d). In addition, the far-field pattern displayed a stable orange-red bright lasing spot, which was visible to the naked eye on the screen under strong excitation power conditions (Fig. 3e). The inset in Fig. 3e shows the hit map of interference fringes obtained using the emitted laser beam *via* a Michelson interferometer, and the high-contrast fringes indicate good coherence of the polariton laser.

For further investigation of the mechanism of polariton BEC lasing in the CQD-microcavity, the temporal dynamic behavior was measured by the time-correlated single-photon counting (TCSPC) method (Fig. 4a and b). The emission dynamics of bare CQDs and CQD-microcavity exhibited the typical exponential decay of lifetime. The green auxiliary lines in Fig. 4a and b represent the corresponding exponential

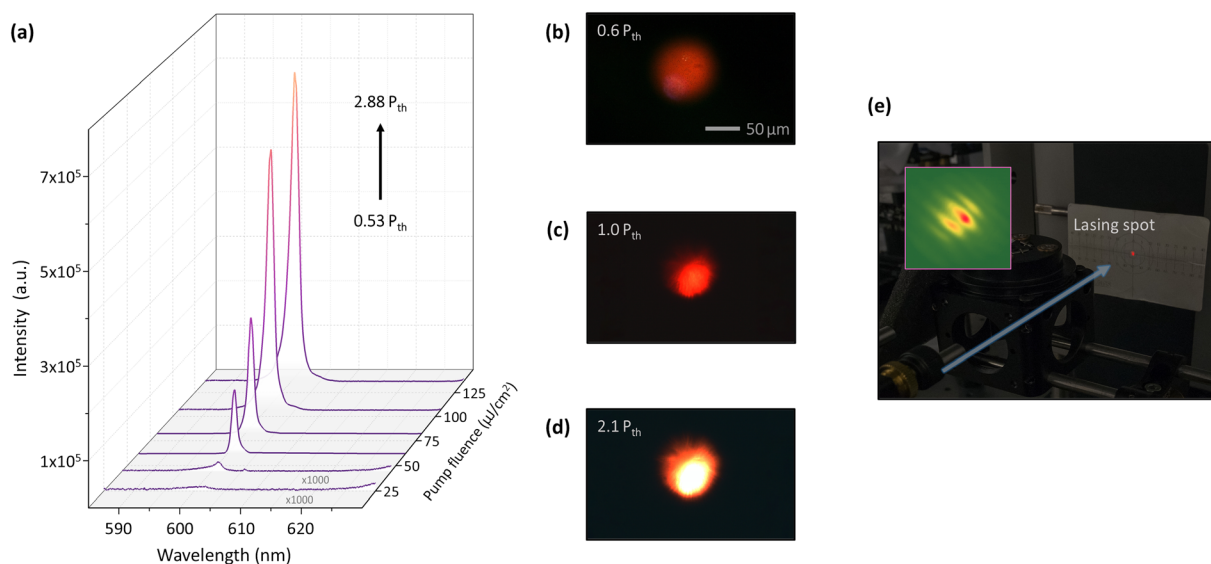


Fig. 3 Features of the CQD-microcavity polariton laser. (a) Emission spectra of the CQD-microcavity integrated over all angles under different excitation densities. (b–d) Near-field emission patterns of the CQD-microcavity at excitation powers of $0.6P_{th}$, $1.0P_{th}$, and $2.1P_{th}$. (e) Far-field image of the output laser beam of the device. Inset: The interference fringe pattern of CQD lasing emission.



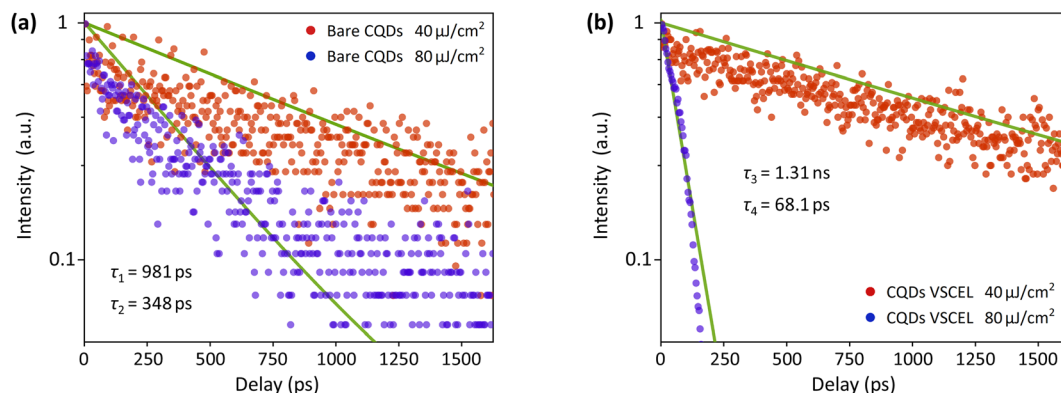


Fig. 4 Temporal dynamics of the CQD-microcavity device. (a) Emission dynamics of bare CQDs at different excitation powers. Due to the coherent amplification effect, the lifetime at higher excitation power (348 ps) is significantly shorter than at lower power (980 ps). The green auxiliary lines indicate the exponential decay fitting. (b) Emission dynamics of the CQD microcavity device at low ($40 \mu\text{J cm}^{-2}$) and high ($80 \mu\text{J cm}^{-2}$) excitation powers. As a result of the formation of polariton coherent radiation, the lifetime of the quasi-particle system is significantly reduced.

fitting results. Although the coherent amplification effect at high excitation powers led to a reduction in emission lifetime from 981 to 348 ps for the bare sample, the lifetimes remain within the same order of magnitude. In contrast, the emission lifetime of the CQD microcavity was 1.3 ns when the excitation power was below P_{th} . However, a significant reduction in emission lifetime (68 ps) was observed as lasing emission occurred, indicating the establishment of coherence-stimulated emission in the polariton quasi-particle system. In other words, the relaxation of polaritons was facilitated by stimulated scattering toward the ground state of LP, which approached the temporal resolution limit of our TCSPC device (50 ps). Notably, the emission lifetime of the CQD-microcavity was longer than that of bare CQDs below P_{th} , which can be attributed to the reflection effect of the pumping pulse by the DBRs.

In previous studies on exciton-polariton lasers, the lasing emission typically exhibits significant linear polarization due to the transverse electric (TE) and transverse magnetic (TM) mode splitting effect inherent to the microcavity lattice orientation.^{16,23} However, this phenomenon is less pronounced in CQDs polariton lasers. The random nature of the colloidal dispersion results in a probabilistic selection between the TE and TM modes, rather than a strict mode coupling mechanism. Consequently, our CQD polariton laser exhibited a low-polarization contrast elliptical polarization both below and above the threshold (Fig. 5a). Specifically, the polarization states showed no significant variation across different excitation powers and aligned with the polarization direction of the cavity transmission, while showing no correlation with the polarization of the excitation laser (Fig. 5b).

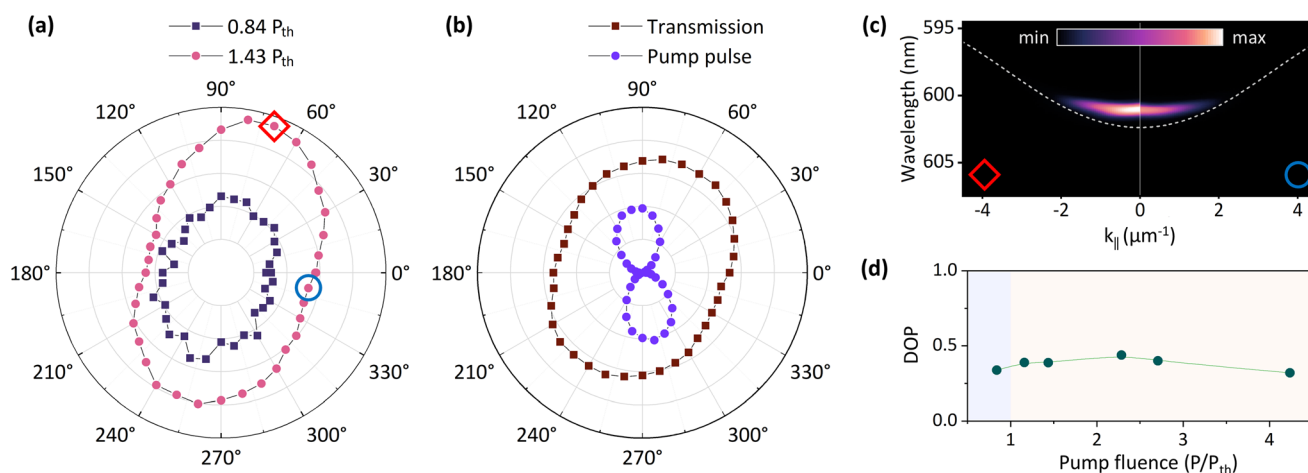


Fig. 5 Polarization characteristics of the CQD-microcavity device. (a) The polarization characteristics of the CQD microcavity show a consistent behavior below and above P_{th} . (b) The polarization characteristics of the microcavity transmission spectra and the linear polarization direction of the pumping laser. (c) Angle-resolved spectra at the polariton laser signal maxima and minima marked in (a). (d) DOP of the CQD microcavity laser under different excitation power values. The elliptical polarization of the device maintains a value of about 0.3–0.4.



Table 1 Comparison of several reported polariton lasing at RT using inorganic materials

Material	Emission wavelength (nm)	Linewidth (nm)	Q-factor	Ref.
ZnO nanobelt	387	0.78	500	20
ZnO microwire	389	0.43	900	22
GaN	371	0.2	1800	24
GaN/AlGaN	346	0.67	520	25
CdSe/ZnSe/ZnS QDs	601	0.65	920	This work

The angle-resolved spectra corresponding to the maximal and minimal polarization intensities of the CQD polariton laser were recorded (Fig. 5c). They evidently showcased that the primary difference between the two states lies in the emission intensity, with no discernible energy splitting detected within the precision limits of the experimental setup. The degree of polarization (DOP) is defined as:

$$\text{DOP} = (I_{\max} - I_{\min}) / (I_{\max} + I_{\min})$$

where I_{\max} and I_{\min} indicate the maximum and minimum emission intensities of the two orthogonal polarization directions. As shown in the spectra, the DOP maintained a value of 0.3 to 0.4 with increasing excitation power (Fig. 5d). This suggests that the limited TE–TM splitting in the microcavity is insufficient to drive the development of pronounced linear polarization, causing the CQD polariton laser to spontaneously undergo elliptical polarization under statistical equilibrium conditions.

Table 1 lists the critical parameters of the condensation lasing of polaritons in RT using different active media. Compared with traditional semiconductor materials, the CQD polariton laser developed in this work exhibited similar linewidth and Q-factor but at a lower fabrication cost as this approach does not require a particular growth substrate.

In summary, we achieved RT polariton BEC lasing using a CdSe-based CQD strong coupling microcavity, with a stable lasing P_{th} of $49 \mu\text{J cm}^{-2}$. The dispersion mappings of the CQD polariton laser provide a rigorous analysis of coherence in the BEC process. The typical energy shift and condensation behavior of the LP branch provide strong evidence for the interaction of bosons. Moreover, the transient dynamic and polarization characteristics of the laser were explored. The robust polariton lasing not only validates the unique properties of the CQD media but also reveals the universal principles of polariton quasi-particles. Compared with previously reported colloidal nanocrystal lasers, this material exhibits superior spectral characteristics and a low excitation threshold. In comparison with other RT polariton lasers, our results demonstrate a lower spontaneous-emission coupling factor and novel polarization properties, representing a worthy complement to existing materials. Further optimizations of CQD synthesis and microcavity design, such as localized structures to form polariton potential traps, are expected to reduce the lasing threshold and enable continuous-wave laser pumping. Our work presents

a promising approach for realizing low-threshold polariton lasers *via* CQDs, offering hope for the practical application of CQD lasers and the development of novel polariton devices.

Experimental section

Synthesis of CdSe/ZnSe/ZnS QDs

Cadmium oxide (0.5 mmol), 1-octadecene (4 mL) and oleic acid (1 mL) were mixed in a 50 mL three-necked flask and heated to 120 °C, and the flask was exhausted under a nitrogen flow for 1 h. After that, the temperature was raised to 310 °C, and 1 mL of the selenium precursor solution was rapidly injected, and the reaction was performed for 10 min to grow CdSe cores. After that, the temperature was lowered to 200 °C, and 2 mL of the zinc precursor solution was added. Then, the temperature was raised to 290 °C, and 2 mL of the selenium precursor was added dropwise for 10 min to grow the ZnSe shell. After that, the temperature was lowered to 200 °C again, and 2 mL of the zinc precursor was added. While coating the ZnS shell layer, the temperature was raised to 280 °C, and then 5 mL of a sulfur precursor was added dropwise for 10 min to grow the ZnS shell. The details of the chemicals and the preparation of the precursor solutions are given in the ESI.†

Optical characterization

In the experiments, the CQD polariton lasing measurement was carried out using a home-built angle-resolved micro-spectroscopy system. A regenerative amplified mode-locked Ti:Sapphire oscillator (Coherent Astrella) with output centered at 800 nm (repetition rate of 1 kHz) was frequency-doubled to generate a near-ultraviolet laser with a pulse width of 100 fs. The emission spectra were analyzed by using a monochromator (HORIBA iHR320) and an electrically cooled CCD (Andor DU970P). The temporal dynamics experiment was performed using a standalone TCSPC module and a fast photomultiplier tube (PicoHarp 300, MPD).

Data availability

All data included in this study are available from the corresponding author upon request.

Conflicts of interest

The authors declare no conflict of interest.

Acknowledgements

We acknowledge financial support from the National Natural Science Foundation of China (No. U22A2073, 62474197), The Guangdong Basic and Applied Basic Research Foundation (2024A1515011536) and the Guangzhou Basic and Applied Basic Research Foundation (2025A04J7142).



References

- 1 P. Bhattacharya and Z. Mi, Quantum-Dot Optoelectronic Devices, *Proc. IEEE*, 2007, **95**(9), 1723–1740.
- 2 J. M. Pietryga, Y. S. Park, J. Lim, A. F. Fidler, W. K. Bae, S. Brovelli, *et al.*, Spectroscopic and Device Aspects of Nanocrystal Quantum Dots, *Chem. Rev.*, 2016, **116**(18), 10513–10622.
- 3 C. R. Kagan, E. Lifshitz, E. H. Sargent and D. V. Talapin, Building devices from colloidal quantum dots, *Science*, 2016, **353**(6302), aac5523.
- 4 M. Asada, Y. Miyamoto and Y. Suematsu, Gain and the threshold of three-dimensional quantum-box lasers, *IEEE J. Quantum Electron.*, 1986, **22**(9), 1915–1921.
- 5 H. C. Chien, C. Y. Cheng and M. H. Mao, Continuous Wave Operation of SiO₂ Sandwiched Colloidal CdSe/ZnS Quantum-Dot Microdisk Lasers, *IEEE J. Sel. Top. Quantum Electron.*, 2017, **23**(5), 1–5.
- 6 F. Fan, O. Voznyy, R. P. Sabatini, K. T. Bicanic, M. M. Adachi, J. R. McBride, *et al.*, Continuous-wave lasing in colloidal quantum dot solids enabled by facet-selective epitaxy, *Nature*, 2017, **544**(7648), 75–79.
- 7 L. Zhang, C. Liao, B. Lv, X. Wang, M. Xiao, R. Xu, *et al.*, Single-Mode Lasing from “Giant” CdSe/CdS Core–Shell Quantum Dots in Distributed Feedback Structures, *ACS Appl. Mater. Interfaces*, 2017, **9**(15), 13293–13303.
- 8 M. M. Adachi, F. Fan, D. P. Sellan, S. Hoogland, O. Voznyy, A. J. Houtepen, *et al.*, Microsecond-sustained lasing from colloidal quantum dot solids, *Nat. Commun.*, 2015, **6**(1), 8694.
- 9 Y. Wang, K. S. Leck, V. D. Ta, R. Chen, V. Nalla, Y. Gao, *et al.*, Blue Liquid Lasers from Solution of CdZnS/ZnS Ternary Alloy Quantum Dots with Quasi-Continuous Pumping, *Adv. Mater.*, 2015, **27**(1), 169–175.
- 10 C. Dang, J. Lee, C. Breen, J. S. Steckel, S. Coe-Sullivan and A. Nurmikko, Red, green and blue lasing enabled by single-exciton gain in colloidal quantum dot films, *Nat. Nanotechnol.*, 2012, **7**(5), 335–339.
- 11 J. Maskoun, N. Gheshlaghi, F. Isik, S. Delikanli, O. Erdem, E. Y. Erdem, *et al.*, Optical Microfluidic Waveguides and Solution Lasers of Colloidal Semiconductor Quantum Wells, *Adv. Mater.*, 2021, **33**(10), 2007131.
- 12 Y. S. Park, J. Roh, B. T. Diroll, R. D. Schaller and V. I. Klimov, Colloidal quantum dot lasers, *Nat. Rev. Mater.*, 2021, **6**(5), 382–401.
- 13 M. Nomura, N. Kumagai, S. Iwamoto, Y. Ota and Y. Arakawa, Laser oscillation in a strongly coupled single-quantum-dot-nanocavity system, *Nat. Phys.*, 2010, **6**(4), 279–283.
- 14 D. Mao, L. Chen, Z. Sun, M. Zhang, Z. Y. Shi, Y. Hu, *et al.*, Observation of transition from superfluorescence to polariton condensation in CsPbBr₃ quantum dots film, *Light: Sci. Appl.*, 2024, **13**(1), 34.
- 15 J. Zhang, C. Li, J. Li and X. Peng, Synthesis of CdSe/ZnSe Core/Shell and CdSe/ZnSe/ZnS Core/Shell/Shell Nanocrystals: Surface-Ligand Strain and CdSe–ZnSe Lattice Strain, *Chem. Mater.*, 2023, **35**(17), 7049–7059.
- 16 Y. Wang, H. Zheng, Z. Tang, R. Wang, X. Luo, Y. Shen, *et al.*, Spin-Polarization-Induced Chiral Polariton Lasing at Room Temperature, *ACS Photonics*, 2023, **10**(6), 1936–1943.
- 17 R. Wang, Y. Wang, H. Zheng, J. Dong, L. Wang, H. Chen, *et al.*, Ultra-Low Threshold Single-Mode Upconversion Lasing in a Strong Coupled Microcavity via Four-Photon Absorption, *Adv. Opt. Mater.*, 2024, **12**(4), 2301637.
- 18 M. S. Skolnick, T. A. Fisher and D. M. Whittaker, Strong coupling phenomena in quantum microcavity structures, *Semicond. Sci. Technol.*, 1998, **13**(7), 645–669.
- 19 V. I. Klimov, S. A. Ivanov, J. Nanda, M. Achermann, I. Bezel, J. A. McGuire, *et al.*, Single-exciton optical gain in semiconductor nanocrystals, *Nature*, 2007, **447**(7143), 441–446.
- 20 Z. Chen, H. Zheng, H. Zhu, Z. Tang, Y. Wang, H. Wei, *et al.*, Robust Polariton Bose–Einstein Condensation Laser via a Strong Coupling Microcavity, *Laser Photonics Rev.*, 2020, **14**(12), 2000273.
- 21 H. Deng, G. Weihs, D. Snoke, J. Bloch and Y. Yamamoto, Polariton lasing vs. photon lasing in a semiconductor microcavity, *Proc. Natl. Acad. Sci. U. S. A.*, 2003, **100**(26), 15318–15323.
- 22 D. Xu, W. Xie, W. Liu, J. Wang, L. Zhang, Y. Wang, *et al.*, Polariton lasing in a ZnO microwire above 450 K, *Appl. Phys. Lett.*, 2014, **104**(8), 082101.
- 23 J. Kasprzak, M. Richard, S. Kundermann, A. Baas, P. Jeambrun, J. M. J. Keeling, *et al.*, Bose–Einstein condensation of exciton polaritons, *Nature*, 2006, **443**(7110), 409–414.
- 24 S. Christopoulos, G. B. H. Von Högersthal, A. J. D. Grundy, P. G. Lagoudakis, A. V. Kavokin, J. J. Baumberg, *et al.*, Room-Temperature Polariton Lasing in Semiconductor Microcavities, *Phys. Rev. Lett.*, 2007, **98**(12), 126405.
- 25 J. Levrat, R. Butté, T. Christian, M. Glauser, E. Feltn, J. F. Carlin, *et al.*, Pinning and Depinning of the Polarization of Exciton-Polariton Condensates at Room Temperature, *Phys. Rev. Lett.*, 2010, **104**(16), 166402.

